scientific reports

Check for updates

OPEN

Dimerization processes for light-regulated transcription factor Photozipper visualized by high-speed atomic force microscopy

Akihiro Tsuji[1], Hayato Yamashita[1]✉, Osamu Hisatomi[2] & Masayuki Abe[1]

Dimerization is critical for transcription factors (TFs) to bind DNA and regulate a wide variety of cellular functions; however, the molecular mechanisms remain to be completely elucidated. Here, we used high-speed atomic force microscopy (HS-AFM) to observe the dimerization process for a photoresponsive TF Photozipper (PZ), which consists of light–oxygen–voltage-sensing (LOV) and basic-region-leucine-zipper (bZIP) domains. HS-AFM visualized not only the oligomeric states of PZ molecules forming monomers and dimers under controlled dark–light conditions but also the domain structures within each molecule. Successive AFM movies captured the dimerization process for an individual PZ molecule and the monomer–dimer reversible transition during dark–light cycling. Detailed AFM images of domain structures in PZ molecules demonstrated that the bZIP domain entangled under dark conditions was loosened owing to light illumination and fluctuated around the LOV domain. These observations revealed the role of the bZIP domain in the dimerization processes of a TF.

Transcription factors (TFs) are essential DNA binding proteins that regulate a wide range of gene expression. Today, as many as ~1600 human TFs[1] and ~48,000 eukaryotic TFs[2] have been identified. They control various cellular functions critical for living organisms, such as cell proliferation, homeostasis, and immune response[3,4]. A eukaryotic TF monomer recognizes short DNA sequences of approximately 6–8 nucleotide pairs. In addition, these short sequences can randomly occur many times in large genomes. Such numerous random occurrences can lead to spurious binding of TFs[5]. To express the right gene at the right location, at the right moment and at the right level, high specificity must be present for the target DNA sequences. Many TFs form dimers to achieve such high specificity[4,6]. This dimer formation doubles the total effective length of the target sequence and greatly increases both the affinity and the recognition specificity of TF binding compared with those of a monomer[7]. For example, the binding affinity of Gal4, a transcriptional activator in yeast, for the target DNA has been reported to be dramatically reduced by deletion of the dimerization domain[8,9]. Thus, elucidating the TF dimerization mechanism is critical for understanding not only the structure–function relationship of TFs but also the general principle of transcription.

TFs are often categorized into families depending on their dimerization domain type. The basic-region-leucine-zipper (bZIP) domain is one type, and forms a major family[5,7]. Many TFs contain an additional dimerization domain conferring specificity in the range of interactions, such as Per–ARNT–Sim (PAS) domains for signal sensing[4,10,11]. One typical PAS domain is the light–oxygen–voltage-sensing (LOV) domain, which has been found in numerous species and extensively studied[12]. The LOV domain is a photoreactive protein module having a chromophore flavin-mononucleotide (FMN), which receives blue light (BL)[13]. Aureochrome-1 (AUREO1) is a TF possessing both the bZIP domain and the LOV domain, and it has been reported to play roles in BL-induced branching and cell proliferation in a stramenopile alga, *Vaucheria frigida*[14–16]. In addition, AUREO1 has been found to dimerize under BL illumination and to bind to the TGACGT target DNA sequence, indicating that this protein is a BL-responsive TF[14,17]. Also a previous study of the isolated LOV domains from AUREO1 revealed the light-induced dimerization[18]. Photozipper (PZ), an N terminally truncated and modified AUREO1, has been

[1]Graduate School of Engineering Science, Osaka University, Osaka, Japan. [2]Graduate School of Science, Osaka University, Osaka, Japan. ✉email: hyama@stec.es.osaka-u.ac.jp

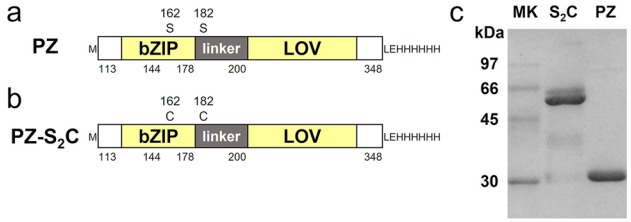

Figure 1. Schematic diagrams and SDS-PAGE of recombinant PZ proteins. (**a**, **b**) Schematic diagrams of the domain structure in PZ and PZ-S_2C. The boundaries of basic region, leucine zipper, linker region, and the LOV domains are indicated by amino acid numbering based on full length AUREO1. Two serine residues in PZ and their substituted cysteine residues in PZ-S_2C are shown with sequence number. (**c**) SDS-PAGE of recombinant proteins under non-reducing conditions: Marker (left lane), PZ-S_2C (center lane), PZ (right lane). The cropped SDS-PAGE is displayed in this figure. The original picture is presented in Supplementary Fig. 1.

constructed for development as an optogenetic tool, and the BL-induced dimerization mechanism has been investigated[17–19]. Size-exclusion chromatography (SEC) and the electrophoretic mobility shift assay revealed that PZ forms a dimer under BL illumination and increases its affinity for the target DNA sequence[17,20]. By studying the bZIP deletion mutant using dynamic light scattering (DLS) and fluorescence resonance energy transfer (FRET), researchers have proposed a model for BL-induced dimerization of PZ[18]. According to the model, the bZIP domain shields the dimerization site of the LOV domain under dark conditions, and the LOV–bZIP intramolecular interaction stabilizes the monomeric form. By contrast, FMN induces conformational changes in the LOV domain upon BL-reception[21–23]. The BL-induced conformational changes in the LOV domain weaken the LOV–bZIP interaction and cause the dissociation of the bZIP domain from the LOV domain. PZ subsequently dimerizes via bZIP–bZIP and LOV–LOV intermolecular interactions through several hydrophobic residues (e.g., F219, V314, V316) on the surface of LOV and bZIP[18,24]. A structural analysis of only the LOV domain in an aureochrome from *Phaeodactylum tricornutum* has clarified the BL-induced conformational changes within the LOV domain[23], and the site-directed mutant studies of PZ have confirmed that the conformational change can affect the LOV–bZIP interaction[19,24]. These studies support some parts of the previously described model. However, in a series of dimerization processes, whole structural arrangement of a PZ molecule remains unrevealed in each state because aureochromes, including PZ, have thus far eluded structural elucidation at full length because of the existence of disordered regions[23,25–27]. In particular, the structural configuration of the bZIP domain in a PZ molecule is speculated to play a key role in the dimer formation[18]. Therefore, a study of the single-molecular structure and dynamics for PZ at full length is necessary.

High-speed atomic force microscopy (HS-AFM) has been extensively used to visualize various biological molecules in physiological solution at nanoscale resolution[28–30]. Notably, HS-AFM observations of intrinsically disordered proteins have revealed flexible and fluctuating unstructured regions[31–33]. These studies have demonstrated that HS-AFM is a useful technique for the single-molecule-level analysis of such proteins containing unstructured segments. Recently, GAL4-VVD, a chimeric fusion construct of a photoresponsive TF[34], has been observed on DNA origami by HS-AFM[35]. Such studies have focused on the dynamics of the fusion protein during the search for the target sites on DNA. However, detailed observations of the TF dimerization process that plays an important role in DNA binding have not been achieved.

Here, we carried out high-resolution observations of the photoresponsive TF "Photozipper" using HS-AFM to elucidate the dimerization mechanism. The HS-AFM images clearly visualized not only the oligomeric states of PZ molecules forming monomers and dimers but also the domain structures within each molecule. Successive AFM movies captured the dimerization process for an individual PZ molecule and the monomer–dimer reversible transition on light–dark cycles. We found that the dimer form is very stable under light conditions compared with the form under dark conditions. The AFM analysis of the domain structures in PZ molecules demonstrated that the bZIP–linker region entangled under dark conditions is loosened because of light illumination. Our results highlight the role of the bZIP domain on PZ dimerization through BL illumination. In addition, they advance understanding of the dimerization mechanism in a TF at the single-molecular level.

Results

Preparation of recombinant PZ proteins. We prepared a recombinant PZ protein by substituting serine for Cys162 and Cys182 in an N-terminally truncated AUREO1 of *Vaucheria frigida* (Fig. 1a). We also prepared a constitutively dimeric mutant protein PZ-S_2C by substituting cysteine for Ser162 and Ser182 in wild-type PZ[36] (Fig. 1b), which has the same amino acid sequence as an N-terminally truncated AUREO1 (with a histidine hexamer at the C-terminal). This S_2C mutant forms a stable dimer irrespective of light conditions by intermolecular disulfide linkages between Cys162 and Cys182 under aerobic conditions and was used for comparing the molecular structure and volume with dimeric PZ. Figure 1c shows the sodium dodecyl sulfate polyacrylamide gel electrophoresis (SDS-PAGE) results for the wild-type PZ and mutant S_2C samples under non-reducing condition. The results for each sample show a single band corresponding to a molecular weight of ~30 kDa for PZ and ~60 kDa for S_2C. These results indicate that each sample was sufficiently pure for use in single-molecule imaging by HS-AFM and that mutant S_2C stably formed the dimer. The S_2C dimer in SDS-PAGE under non-reducing conditions was also reported in a previous study[17].

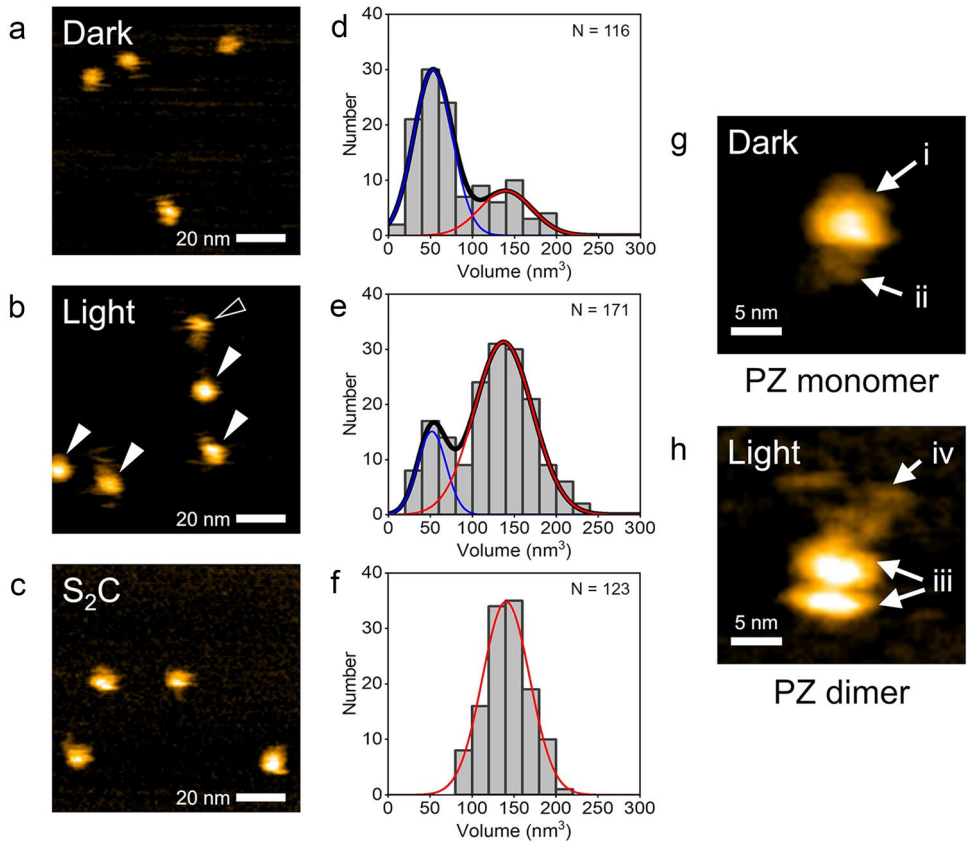

Figure 2. HS-AFM observations of PZ molecules. (**a, b**) HS-AFM images of PZ molecules observed under dark and light conditions, respectively. An open arrowhead indicates the smaller molecule with sizes of ~ 5 nm and filled arrowheads indicate larger ones of ~ 10 nm. (**c**) HS-AFM image of mutant protein PZ-S_2C observed under light conditions. These show still images of successive AFM movie. See also Supplementary Movies 1, 2 and 3. Several PZ and PZ-S_2C molecules were observed on mica surface. (**d**–**f**) Histograms for the molecular volumes analyzed from AFM images of wild-type PZ under dark, light condition and S_2C mutant. N indicates the number of different molecules analyzed for each histogram. Curve represents the fit to a Gaussian distribution. Mean value of each Gaussian curve: (**d**) 1st peak = 52.9 nm^3, 2nd peak = 139 nm^3, (**e**) 1st peak = 52.4 nm^3, 2nd peak = 137 nm^3, (**f**) 141 nm^3. (**g**) Highly magnified AFM image of PZ monomer under dark conditions. This molecule was included in the major distribution in (**d**). The folded-string structure was seen around the spherical structure. (**h**) Highly magnified AFM image of PZ dimer under light conditions. This molecule was included in the major distribution in (**e**). The dimer exhibited a bilobed structure together with the tail-like structure. Protein concentration: (**a**) 25 nM, (**b**) 50 nM, (**c**) 20 nM. Scan ranges: (**a**–**c**) 100 × 100 nm^2, (**g**, **h**) 24.5 × 24.5 nm^2. Scan rates: (**a**, **g**) 1 s/frame, (**b**, **c** and **h**) 0.5 s/frame. Height scales: (**a**) 2.5 nm, (**b**) 3.5 nm, (**c**) 4.3 nm, (**g**) 2.1 nm, (**h**) 2.5 nm.

HS-AFM observations of PZ molecules. We observed the purified PZ molecules using HS-AFM under dark and light conditions in the buffer solution described in the methods section. Figure 2a shows a still image from a successive HS-AFM movie for wild-type PZ captured under dark conditions (Supplementary Movie 1). Globular-shaped molecules ~ 5 nm in diameter were visualized in the AFM image. They were well dispersed and moved rapidly on the mica surface (see also Supplementary Movie 1. The diffusing motions of the molecules will be further discussed in Fig. 3). Occasionally, molecules ~ 10 nm in diameter were also observed (see Supplementary Fig. 2). Figure 2b shows a still image of the HS-AFM movie for wild-type PZ captured under continuous BL illumination (Supplementary Movie 2). Globular-shaped molecules with two diameters were observed in the AFM image. The smaller ones were ~ 5 nm in diameter, and the larger ones were ~ 10 nm. The smaller ones rapidly diffused on the mica surface, whereas the larger ones slowly diffused (see also Supplementary Movie 2). In this HS-AFM movie, a tail-like structure was observed to fluctuate around a globular structure in the larger molecules. To compare these molecular structures with the stable PZ dimer, we observed dimeric mutant protein S_2C using HS-AFM. Figure 2c shows a HS-AFM image of the mutant S_2C molecules under light conditions. The globular molecules were observed, and they exhibited similar diameters to the larger molecules of wild-type PZ under illumination. These molecules slowly diffused on the mica surface (Supplementary Movie 3). In contrast to wild-type PZ, the smaller molecules were not observed in the HS-AFM movie of mutant S_2C. We also observed S_2C molecules under dark conditions and obtained similar results to that of light (Supplementary Fig. 3). To quantitatively compare these results, we analyzed the volumes of the molecules in the HS-AFM images. Figure 2d–f shows histograms for the molecular volumes analyzed from the HS-AFM images of

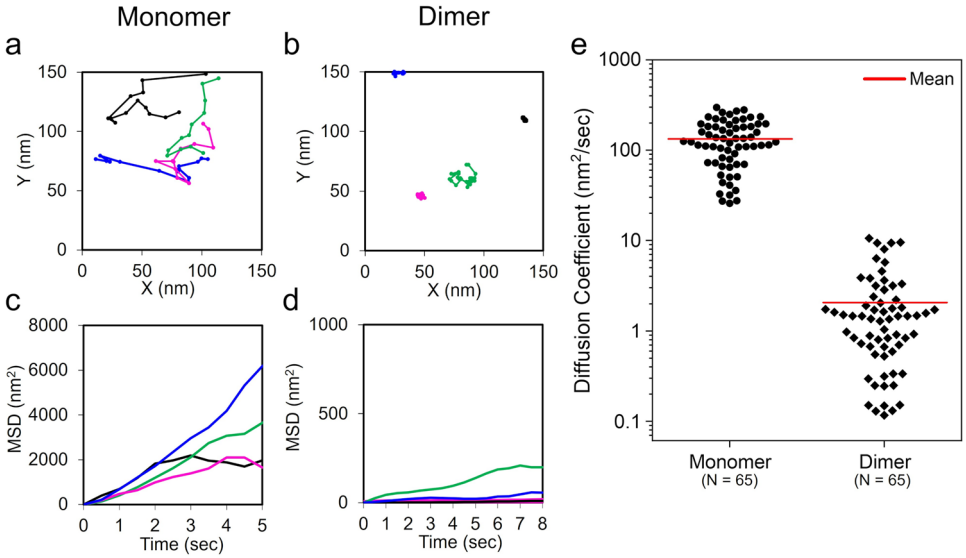

Figure 3. Diffusion analysis of PZ monomer and dimer. (**a**) Molecular trajectories of the two-dimensional diffusion for PZ monomers on mica surface under dark conditions. Four PZ monomers are shown in this graph, which were chosen from the major distribution in Fig. 2d. The mass center position of each PZ molecule was analyzed and tracked in Supplementary Movie 5. (**b**) Molecular trajectories of the two-dimensional diffusion for PZ dimers under light conditions. Four PZ dimers are shown in this graph, which were chosen from the major distribution in Fig. 2e. The mass center position of each PZ molecule was analyzed and tracked in Supplementary Movie 6. (**c**, **d**) Mean square displacements (MSD) analyzed from individual trajectories of (**a**) and (**b**), respectively. These MSD linearly increased with time, yielding diffusion constants. (**e**) Beeswarm plots of diffusion constants analyzed from individual trajectories. Mean value of each distribution: (Monomer) 1.3×10^2 nm^2/s, (Dimer) 2.1 nm^2/s. T-test: $P < 10^{-21}$. Protein concentration: (**a**, **b**) 13 nM.

wild-type PZ under dark and light conditions and from the images of mutant S_2C. The histograms of wild-type PZ under dark conditions (Fig. 2d) and light conditions (Fig. 2e) show bimodal distributions, whereas those of mutant S_2C show unimodal distributions (Fig. 2f, Supplementary Fig. 3). The mean volumes of the mutant S_2C under dark and light conditions were similar to that of the major distribution with higher volumes of wild-type PZ under light conditions. In addition, the mean volume of the major distribution of wild-type PZ under dark conditions was similar to that of the minor distribution with lower volumes of wild-type PZ under light conditions. Therefore, we conclude that the major molecules observed under dark conditions are PZ monomers and that the larger molecules observed under light conditions are PZ dimers. Here, we note that the minor distribution of the larger molecules is seen in Fig. 2d. These molecules are dimers under dark conditions. The results of volume analyses also show that PZ predominantly exists as a monomer under dark conditions and as a dimer under light conditions. These results are consistent with a previous study involving SEC[18], which revealed oligomeric states of PZ under each condition. Thus, we demonstrated that PZ monomers and dimers can be distinguished by HS-AFM. The mean volume ratio of the monomer to dimer was around 1:2.6, which differs slightly from the expected ratio of 1:2 due to dimerization. We could not clarify the major cause of this difference, but the fast diffusion of the monomer might have affected its molecular volume analysis. However, our conclusion that monomers and dimers can be distinguished by HS-AFM is not affected.

We next focused on the structures of the PZ molecules. Figure 2g shows a magnified HS-AFM image of a PZ monomer under dark conditions. This molecule is included in the major distribution in Fig. 2d. Two discernible structural domains of the PZ molecule are observed in the HS-AFM image: a "spherical structure" and a "folded string-like structure," as indicated by labels "i" and "ii" in Fig. 2g, respectively. As shown in Fig. 1a, PZ is composed of two main structural domains: LOV and bZIP, which are connected by a linker region. Previous crystal-structure analyses have revealed that the LOV domain in AUREO1 is spherical, consisting of α-helices and β-sheets[23,25]. Therefore, the spherical structure in our AFM image is thought to be the LOV domain. Furthermore, we deduce that the folded string-like structure in the AFM image is both the bZIP domain and the linker region (bZIP-linker region). Analyses by circular dichroism (CD) spectroscopy and nuclear magnetic resonance (NMR) spectroscopy have shown that the bZIP domain partially forms α-helices in a DNA unbound state[20,37,38]. However, the other structures except for the α-helices remain unrevealed in the bZIP-linker region, although some structural studies have been reported[23,27]. This situation implies that their unknown structures could be disordered in the DNA unbound state[25,27]. In the present study, we visualized the total architecture of the bZIP-linker region under dark conditions for the first time.

Fig. 2h shows a magnified HS-AFM image of a PZ dimer under illumination, which is included in the major distribution in Fig. 2e. Two discernible structural domains of the PZ molecule are evident in the HS-AFM image: a "bilobed structure" and a "fluctuating tail-like structure," as indicated by labels "iii" and "iv" in Fig. 2h, respectively. Previous SEC studies of isolated LOV domains have suggested that the LOV domain dimerizes

under illumination[18,22]. Also, a previous crystal-structural analysis revealed that two LOV domains pair as a dimer under illumination[23]. Therefore, the bilobed structure in our AFM image is thought to be the dimerized LOV domain. The size of the bilobed structure is actually larger than that of the LOV domain in PZ monomers. Here, we note that such dimerized structures of the LOV domains were observed within the fluctuation of the molecules (see Supplementary Fig. 4 and Supplementary Movie 4). Also, such dimerized structures were seen at several scan rates in different dimeric PZ molecules, in which the LOV domains were oriented in various directions (see Supplementary Fig. 5). On the other hand, it is found that the fluctuating tail-like structure in the AFM image is the bZIP-linker region. In a previous study, SEC and FRET analyses revealed that bZIP domains of wild-type PZ also dimerize under illumination[18]. Although we could not resolve bZIP domains dimerizing in our HS-AFM observations, our AFM movies revealed for the first time that they were unexpected flexible structures that fluctuate around the LOV domain (Supplementary Movie 2).

Dynamic movement analysis of PZ molecules. The HS-AFM movies showed obvious differences in not only the molecular size but also the dynamic behavior of PZ molecules under dark and light conditions. PZ monomers rapidly diffused on a mica surface under dark conditions (Supplementary Movie 5). By contrast, PZ dimers fluctuated, exhibiting slow diffusion under illumination (Supplementary Movie 6). To compare these dynamic behaviors, we analyzed the trajectories of PZ molecules in AFM movies. Representative trajectories of PZ monomers under dark conditions and PZ dimers under illumination are shown in Fig. 3a and b, respectively. These PZ molecules exhibited random movements, indicating that the movements are not the effect of a tip–sample interaction force but rather molecular diffusion on the mica surface in a buffer solution. The diffusion speeds of the PZ molecules were quantified by calculating the mean-square displacements (MSDs) for each trajectory. As shown in Fig. 3c and d, each MSD linearly increases with time. In our HS-AFM observations, PZ molecules diffused in two dimensions on the mica surface. Therefore, the MSD plots can be fitted with the following equation for two-dimensional random diffusion[39]:

$$MSD(t) = 4Dt \tag{1}$$

where t is time and D is the diffusion coefficient. The diffusion coefficients for individual PZ molecules are shown in Fig. 3e. The average diffusion coefficient of the dimer was approximately 70 times lower than that of the monomer. This work represents the first observation of the dynamic behavior of each PZ molecule under dark and light conditions using HS-AFM. In a previous study based on DLS, the hydrodynamic radii (R_H) of PZ molecules were measured under dark and light conditions[18]. From the R_H values according to the Stokes–Einstein relationship, we estimated that the diffusion constants are 77 $\mu m^2/s$ under dark conditions and 63 $\mu m^2/s$ under light conditions[40]. This result suggests that the diffusion speeds of PZ molecules decreased upon light-induced dimerization. Our result is consistent with the results of the previous study showing that the diffusion coefficient of the PZ dimer is lower than that of the PZ monomer[18]. It should be noted that the two-dimensional mobility of PZ molecules on the mica surface is much lower than the three-dimensional mobility estimated from previous biophysics experimental data[18,41]. The interaction of PZ molecules with the mica substrate can affect the diffusion speed. Moreover, the average diffusion coefficient of the PZ monomers differed significantly from that of the dimers in the present study, and the diffusion coefficient of the dimers is massively slower than that of the monomers. Although we could not elucidate the major cause of the large difference, the present data suggest a dimer-specific interaction of PZ with the mica substrate. We presume that the molecular conformational change and the change in surface electrical charge due to the dimer formation of PZ molecules may contribute to the specific interaction with the mica substrate. We also note that an aligned orientation of LOV domains in the dimer form on the mica surface can affect the interaction with the mica substrate.

Photoinduced transition process for PZ molecules from monomer to dimer. To investigate the dynamic transition process from PZ monomers to dimers, we conducted successive HS-AFM observations of PZ molecules as the conditions were changed from dark to light. Figure 4a shows snapshots of a successive HS-AFM movie (Supplementary Movie 7). Before BL illumination, PZ monomers were predominant and highly diffusing on the mica surface (dark in Fig. 4a). After BL illumination, the number of PZ dimers increased with time (HS-AFM images from 140 to 342 s in Fig. 4a) and the diffusion speed on the mica surface decreased upon dimer formation (see also Supplementary Movie 7). Finally, PZ dimers became predominant in the AFM image at 390 s. In these successive AFM measurements, we observed the transition processes for PZ molecules from monomers to dimers. Figure 4b shows snapshots of high-magnification AFM images captured during the dimerization processes under BL illumination. Two PZ monomers were diffusing on the mica surface, as shown in the AFM images at 0 s and 2.5 s in Fig. 4b. These monomers collided with each other and formed a single dimer in the AFM image at 4 s. After the molecular collision, the PZ dimer remained bound at 7.5 s (see also Supplementary Movie 8).

We analyzed the number of monomers and dimers at each time point in the successive AFM movies to investigate the kinetics of such a transient response to illumination. Figure 4c shows time courses of each ratio of monomers and dimers among total molecules. Under dark conditions before BL illumination, the monomer ratio was predominant. Moreover, each ratio of monomers and dimers remained constant at different time points. This result indicates that the monomer and the dimer were in equilibrium. After BL illumination, the dimer ratio gradually increased with time, whereas the monomer ratio decreased with time. The dimer ratio exceeded the monomer ratio at ~60 s. Finally, each ratio became saturated, and the dimer ratio was predominant under continuous-light conditions. These results indicate that the equilibrium of PZ transitioned from dark state to light state because of BL illumination (see also Supplementary Note). The transient change of monomers and dimers in such an equilibrium shift can be described as Eqs. (12) and (13), respectively, in the Supplementary Note.

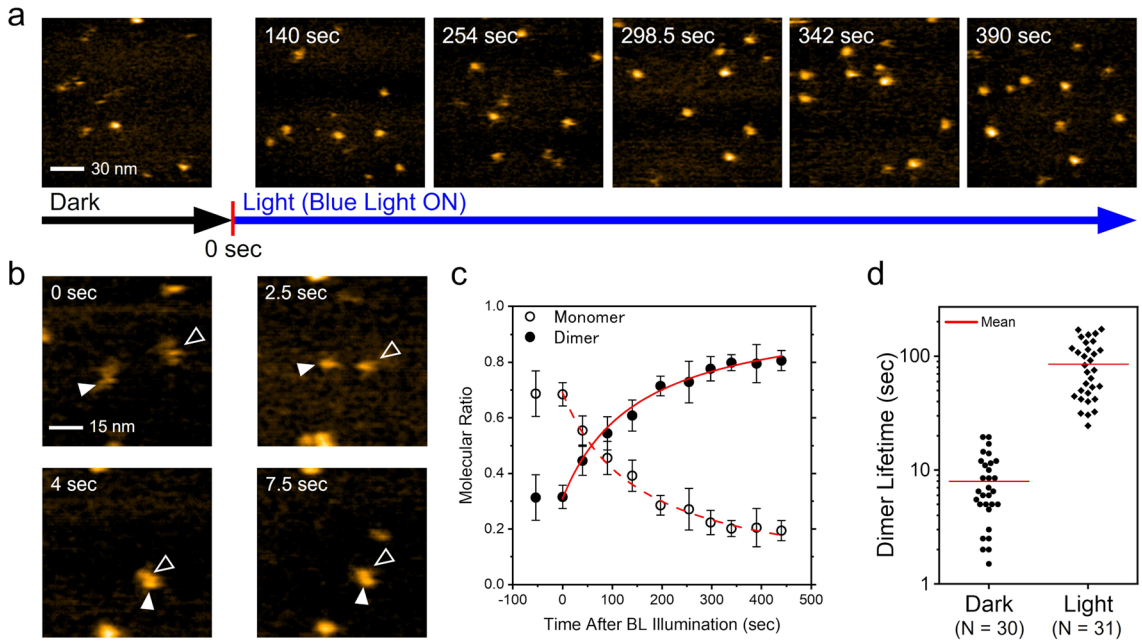

Figure 4. Photoinduced transition process of PZ molecules from monomer to dimer observed by HS-AFM. (**a**) HS-AFM observation of photoinduced transition process of PZ molecules from dark to light state. Time displays in AFM images indicate time course after blue light (BL) illumination. The number of PZ dimers increased with time (see also Supplementary Movie 7). (**b**) Snapshots of successive high magnification AFM movie captured dimerization processes of PZ molecules under BL illumination (Supplementary Movie 8). Two PZ monomers were diffusing on mica surface at 0 s and 2.5 s. Each open and filled arrowheads indicate individual PZ monomers. At 4 s, two PZ monomers collided with each other and formed one dimer. The dimer remained bound at 7.5 s. (**c**) Time courses of each ratio of monomer and dimer detected in AFM images. Each ratio was normalized by the total PZ molecules in each AFM image. Note that one PZ dimer was counted as two PZ molecules. Open and filled circles indicate average ratio of monomer and dimer, respectively (N = 3). Error bars indicate the standard deviation. These plots were fitted with Eqs. (12) and (13) in the Supplementary Note, respectively (red solid line and dotted line). (**d**) Beeswarm plots of dimer lifetimes of PZ molecules under dark and light conditions. These data were analyzed from successive AFM measurement before and after light illumination. Mean value of each distribution: (Dark) 8.1 s, (Light) 86 s. T-test: $P < 10^{-9}$. Protein concentration: (**a**, **b**) 38 nM. Scan ranges: (**a**) 150×150 nm^2, (**b**) 75×75 nm^2. Scan rates: (**a, b**) 0.5 s/frame. Height scales: (**a, b**) 3.5 nm.

Our data were well fitted with these equations, as shown by solid and dashed curves in Fig. 4c. The time constant (τ) of the dimerization rate was 255 ± 26 s, as calculated using Eq. (14) in the Supplementary Note. A previous study that used a transient grating (TG) method revealed that the time constant of PZ dimerization was 2 s at a PZ concentration of 20 μM[41]. This concentration is three orders of magnitude higher than ours (38 nM). The PZ dimerization speed depends on the PZ concentration[41]: a high concentration leads to a low time constant (see Eq. (14) in the Supplementary Note). Therefore, our low PZ concentration is considered to result in an increase of the time constant. The concentrations of typical TFs in cells are known to be on the order of 10–100 nM[42–44]. We successfully measured the PZ behavior by HS-AFM under concentration conditions similar to the concentrations in cells. It should be noted that the diffusion speed of PZ molecules is lower in our measurements owing to the interaction between the PZ and the mica substrate. Here, we performed successive HS-AFM measurements of PZ kinetics in repeated light–dark cycles to confirm the reproducibility of the photoinduced transition between the monomers and dimers (Supplementary Fig. 6). The initial BL responses were approximately the same as that in Fig. 4c. Under dark conditions, after the initial BL illumination, the dimer ratio gradually decreased with time, whereas the monomer ratio increased with time. At ~ 1300 s, each PZ ratio returned to the initial state. Similar responses were reproduced in the second light–dark cycle. Therefore, these results indicate that such a photoinduced monomer–dimer transition of PZ is a reversible process. We demonstrated that HS-AFM can reproducibly capture the physiological behavior of PZ at the single-molecule level.

Successive HS-AFM movies captured not only the processes of dimer formation but also that of dissociation (see Supplementary Fig. 7 and Supplementary Movie 9). Through these measurements of the photoinduced transition processes, we noticed an interesting difference in that the PZ dimer formation is very stable under BL illumination compared with that under dark conditions. We therefore analyzed the lifetimes from dimer formation to dissociation. Figure 4d shows the dimer lifetimes under dark and light conditions. Notably, these dark dimers are not in a transient state but in a steady state under dark conditions. The average dimer lifetime under illumination (86.0 s) was 10 times longer than that under dark conditions (8.1 s). This result suggests that the intramolecular interaction of the PZ dimer (monomer–monomer intermolecular interaction) under BL illumination is much stronger than that under dark conditions. This work is the first report directly comparing the

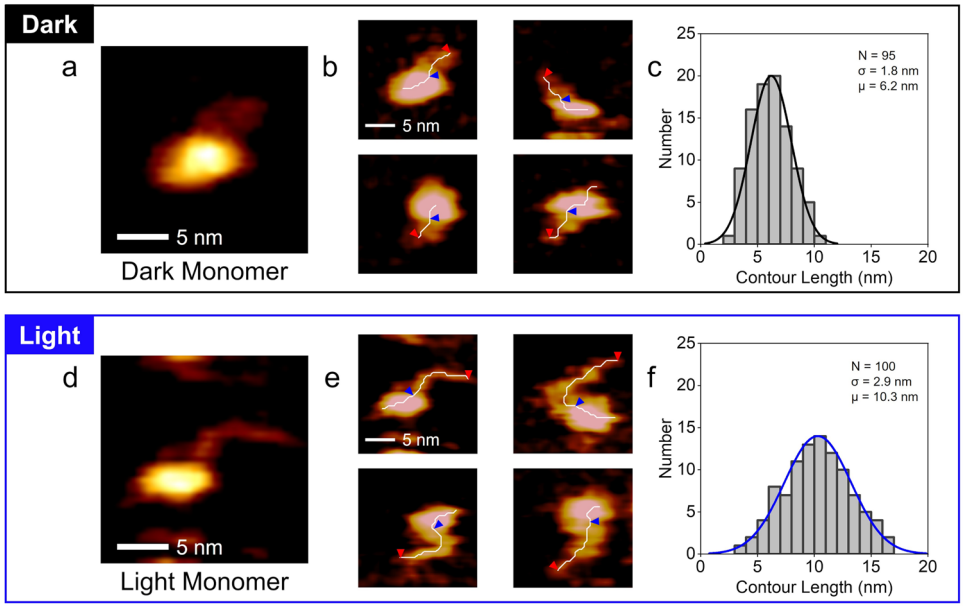

Figure 5. HS-AFM observations of PZ molecules under dark and light conditions. (**a**) Typical HS-AFM image of PZ monomer under dark conditions. (**b**) HS-AFM image gallery of PZ monomers under dark conditions. A skeleton line is drawn in white on each PZ monomer. Red and blue arrowheads show each end of the bZIP-linker region in PZ monomer (see Methods and Supplementary Fig. 8). The lengths of the skeleton lines between red and blue arrowheads were analyzed as the contour lengths of the bZIP-linker region. (**c**) Histograms for the bZIP-linker contour lengths analyzed from AFM images of PZ monomers under dark conditions. Curve represents the fit to a Gaussian distribution. The mean value of the Gaussian curve: $\mu = 6.2$ nm. (**d**) Typical HS-AFM image of PZ monomer under light conditions. (**e**) HS-AFM image gallery of PZ monomers under light conditions. The skeleton lines and the contour lengths were analyzed by same procedures as (**b**). (**f**) Histograms for the bZIP-linker contour lengths analyzed from AFM images of PZ monomers under light conditions. The mean value of the Gaussian curve: $\mu = 10.3$ nm. T-test for (**c**) and (**f**): $P < 10^{-22}$. For (**c**) and (**f**), N indicates the number of different molecules analyzed for each histogram. Protein concentrations: (**a**–**c**) 13 or 25 nM, (**d**–**f**) 25 or 50 nM. Scan ranges: 20×20 nm^2, Scan rates: 0.5 s/frame. Height scales: (**a**) 3.6 nm, (**b**) top-left: 3.6 nm, top-right: 2.5 nm, bottom-left: 2.1 nm, bottom-right: 3.4 nm, (**d**) 1.8 nm, (**e**) top-left: 1.8 nm, top-right: 1.7 nm, bottom-left: 1.4 nm, bottom-right: 2.0 nm.

stability of each PZ dimer molecule under dark and light conditions. We note that, as described in the previous section, the PZ dimers can specifically interact with the mica substrate, but they don't affect our conclusion in Fig. 4d because both the dimers under dark and light condition are equally affected by the interaction.

Light-induced conformational change of PZ monomers. We found that the PZ dimer is more stable under BL illumination than under dark conditions. This increase in dimer stability is attributed to the conformational change of PZ molecules under illumination. To reveal the mechanism of dimer stabilization, we focused on the molecular structure of the PZ monomer under light and dark conditions. Figure 5a shows a magnified HS-AFM image visualizing the detailed structure of a PZ monomer under dark conditions. As described in Fig. 2g, the spherical structure corresponds to the LOV domain and the folded string-like structure corresponds to the bZIP-linker region. Figure 5b shows a HS-AFM image gallery of the PZ monomers under dark conditions. The structure of each monomer is similar to that in Fig. 5a, and such structures were also confirmed for the other monomers under dark conditions. Figure 5d shows a magnified HS-AFM image of a PZ monomer under illumination. Surprisingly, an unfolded string-like structure anchored to the spherical LOV domain is visualized in this detailed HS-AFM image. Figure 5e shows a HS-AFM image gallery of PZ monomers under illumination. The structure of each monomer was similar to that in Fig. 5d, and these structures appeared to wobble on the mica surface. Such structures were also confirmed for the other monomers under light conditions. These results suggest that the illumination changed the conformation of the PZ monomers.

To investigate the conformational change of the PZ, we analyzed the contour lengths of string-like structures in the PZ monomers, as shown by white lines and two arrowheads in Fig. 5b and e (see also Methods and Supplementary Fig. 8). Figure 5c and f show the histograms for the contour lengths analyzed from the HS-AFM images of the PZ monomers under dark and light conditions, respectively. The mean value of the contour lengths under illumination (10.3 nm) was 1.7 times longer than that under dark conditions (6.2 nm). In addition, the distribution of the contour lengths under illumination ($\sigma = 2.9$ nm) was wider than that under dark conditions ($\sigma = 1.8$ nm). These results indicate that the string-like structure that was folded under dark conditions was unfolded under illumination and then fluctuated in solution. Thus, we conclude that the bZIP-linker region entangled under dark conditions is loosened under illumination.

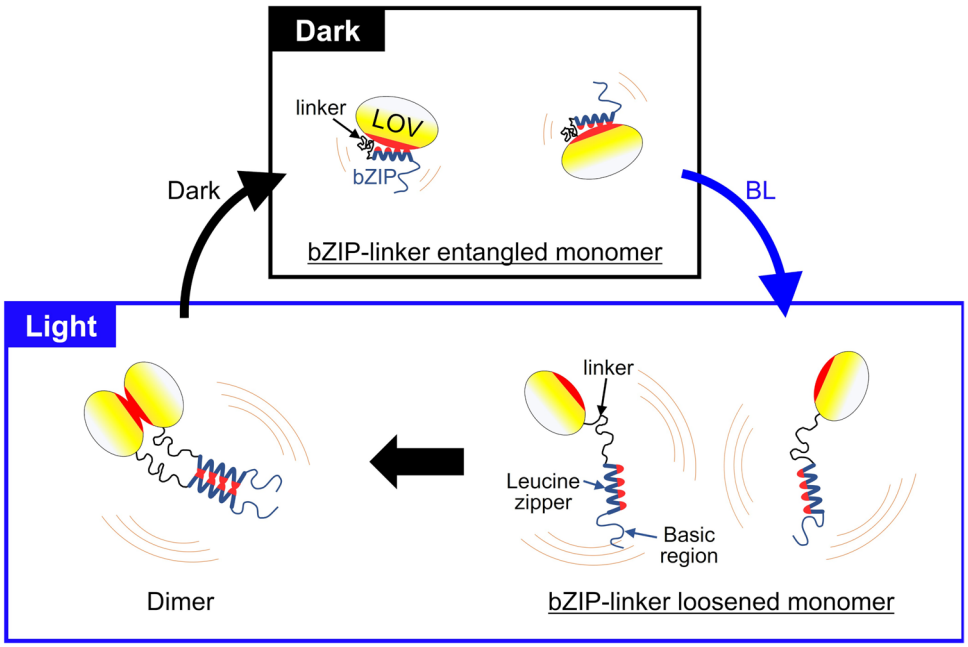

Figure 6. Schematic model of the BL induced dimerization process of Photozipper. Under dark conditions, PZ exists as a bZIP-linker entangled monomer where the hydrophobic dimerization sites (red colored areas) are hidden by the bZIP–LOV intramolecular interaction. Such molecular configuration of PZ inhibits the dimerization under dark conditions. BL induces the dissociation of the bZIP from the LOV surface and the dimerization sites become exposed (lower-right). The loosened and elongated bZIP-linker fluctuates around the LOV. This flexible and dynamic movement of bZIP increases the contact with the other monomers and facilitates the dimerization. The intermolecular interaction of LOV–LOV and bZIP–bZIP stabilize the PZ dimer (lower-left).

Discussion

We observed the single-molecular structure and dynamics of PZ in physiological buffer solution using HS-AFM under controlled dark–light conditions. The HS-AFM images show monomer dominance under dark conditions and dimer dominance under light conditions. HS-AFM movies captured the dimerization process for individual PZ molecules and the monomer–dimer reversible transition during dark–light cycles. For the first time, HS-AFM was used to visualize detailed structures of PZ and revealed the structural configuration of the bZIP domain in the full-length PZ molecule in both the light state and the dark state. These results demonstrate the validity of the previous PZ dimerization model[18] and update details of some aspects of the model, as described in Fig. 6.

In the dark state, the bZIP-linker region is entangled and interacts with the LOV domain. Here, we consider that the bZIP domain binds to the LOV domain, hiding the dimerization sites of both the LOV domain and the bZIP domain, as previously reported[23]. Therefore, the dimerization with the other PZ monomer is inhibited under dark conditions. Indeed, we found that the binding lifetime of the formed dimer was very short under dark conditions compared with that under illumination (Fig. 4d). Thus, the bZIP domain and the LOV domain play a role in mutual autoinhibition of PZ dimerization in the dark state. By contrast, the BL-induced conformational changes in the LOV domain lead to the dissociation of the bZIP domain from the LOV surface (Fig. 6). We successfully visualized the loosening and elongation of the bZIP domain under BL illumination. In addition, we revealed that the elongated bZIP domain fluctuates around the LOV domain (Fig. 5). The structure of the leucine zipper in the bZIP domain has been determined as an α-helix by various techniques, whereas the supposedly unfolded basic and linker region in the DNA-unbound state lacks the structural details up to date (Fig. 6)[23,27,45]. Since we could measure the length of the bZIP-linker region by HS-AFM in this study, to obtain further information for the unrevealed basic and linker regions, we compared our HS-AFM results with the presumable length of the bZIP-linker in PZ. The length was estimated on the basis of several literature as follows. The length of an unfolded amino acid (aa) chain can be described as $L = (N_{aa} - 1) \times d_{aa}$, where N_{aa} is the number of aa, and d_{aa} is the average distance between two aa, which is most likely 0.36 nm[33,46]. Also, a turn of a typical α-helix contains 3.6 residues with a length of 0.54 nm[47]. If the basic and linker regions are completely unfolded, from the number of aa contained in each region of PZ (Fig. 1a), the bZIP-linker region will be roughly estimated to be ~ 24.1 nm. The average length of the region measured by HS-AFM as shown in Fig. 5f was 10.3 nm, which was less than half of the estimated one. This suggests that the bZIP-linker region of PZ will contain largely folded structures in the basic and linker regions but not completely unfolded structures (lower right in Fig. 6). This direct visualization and quantification of such dynamic behavior of the domain structures in TFs have ever been unachieved with any other techniques and was realized by HS-AFM for the first time in the present study.

The fast diffusion of PZ monomers can increase collisions with other monomers (Fig. 3). In addition, the elongation and fluctuation of the bZIP domain can increase contact with other monomer because such a bZIP domain can have a greater capture radius for a specific binding site than the entangled state with restricted conformational freedom. This dynamic behavior of the bZIP domain is considered to contribute to the rapid formation of the stable dimer (Fig. 6). Previous studies on bZIP have proposed the fly-casting mechanism, where the fluctuation of a flexible bZIP domain accelerates the search for specific target DNA[48,49]. Our results suggest that this mechanism can also be extended to TF dimerization processes. Thus, PZ dimerization is accurately regulated by the autoinhibition due to the intramolecular interaction and is facilitated by the dynamic fluctuation of the flexible bZIP domain because of the BL-induced conformational change. Such autoinhibition due to intramolecular interactions has also been suggested for the other TFs[50,51]. Activating transcription factor 2 (ATF2)[52,53] and CCAAT/enhancer binding protein-β (CEBPB)[54,55] are examples of medically important TFs involved in various diseases such as cancer-cell multiplications and inflammatory processes. We expect HS-AFM to be useful for studying the unknown regulatory mechanism of such TFs through visualization of the domain structures and the corresponding single-molecular dynamics. Moreover, this technique is widely expected to be applicable for observing DNA-binding processes of TFs. In conclusion, we have revealed the significant role of the bZIP domain in the dimerization process for the photoresponsive TF Photozipper. Our results demonstrate the enormous potential of HS-AFM imaging for transcriptional studies.

Methods

Sample preparation. Recombinant wild-type PZ and mutant S_2C proteins with His-tags on C-termini were prepared as described previously[17]. In brief, *Escherichia coli* cells expressing recombinant PZ proteins were harvested by centrifugation and disrupted by sonication. After the cell debris was removed by centrifugation, recombinant proteins were purified twice by binding to and eluting from a Ni Sepharose 6 Fast Flow column (GE Healthcare) and a HiTrap Heparin HP column (GE Healthcare) according to the manufacturer's instructions. The recombinant proteins were stored at 4 °C in a solution (Buffer-A) containing 400 mM NaCl, 20 mM Tris–HCl (pH 7.0), 1 mM dithiothreitol (DTT), and 0.2 mM phenylmethylsulfonyl fluoride (PMSF). The purity of the PZ recombinant proteins was confirmed by SDS-PAGE under non-reducing conditions, and the concentrations of the recombinant proteins were determined from the absorbance at 447 nm using an extinction coefficient of 13,000 M^{-1} cm^{-1}[17]. Samples for HS-AFM observations were diluted in a solution (Buffer-B) containing 1 mM NaCl, 20 mM Tris–HCl (pH 7), 1 mM DTT, and 0.2 mM PMSF.

HS-AFM observation of PZ molecules

Imaging was performed with a laboratory-built HS-AFM apparatus, which is an improved version of the previously reported AFM[56]. The HS-AFM apparatus was installed in a darkroom. HS-AFM images were acquired using tapping mode. To detect cantilever deflection, we used an optical beam deflection detector equipped with an infrared laser (980 nm) to avoid exciting the PZ. The laser beam was focused onto a small cantilever [$0.1 \le k \le 0.2$ N/m, $800 \le f \le 1200$ kHz in solution (Olympus), where k is the spring constant and f is the resonant frequency] using a 40 × objective lens. The AFM styli were placed on each cantilever by electron-beam deposition and were sharpened by plasma etching. A 1.5 mm-diameter mica disk was glued onto a sample stage made of quartz glass. A sample droplet with a volume of 1.5 μL was placed on the freshly cleaved mica surface and incubated for 3 min. The mica surface was then rinsed with Buffer-B solution. These preparations for HS-AFM imaging were conducted under dim red light to avoid exciting the PZ for the experiments under dark conditions. In contrast, those sample preparations were conducted under blue LED light (450 nm) for the experiments under light conditions. HS-AFM measurements were performed in Buffer-B solution at room temperature. For the photoexcitation of PZ samples during HS-AFM imaging, blue laser (450 nm) irradiation was performed through a 40 × objective lens. The intensity measured at the exit of the objective lens was approximately 2 mW and the power density applied to the samples was estimated to be approximately 4.3 mW/mm^2.

Data analysis of HS-AFM images

The molecular volume and the mass center position of each imaged PZ molecule were analyzed using the following procedures. First, a Gaussian filter was applied to the HS-AFM images to reduce noise. Second, the grayscale of the images was digitized using a threshold determined by the half-maximum height to detect the boundary of a PZ molecule. The pixels with grayscales greater than the threshold were defined as the PZ molecular region (region of interest; ROI). The molecular volume of a PZ molecule was calculated by integrating the volume of each pixel within the ROI. Histogram analyses were performed using the volumes from different molecules (N indicates the number of the analyzed different molecules). AFM molecular images containing image artifacts due to massive fast molecular motions were not used for the analyses. Ideally, AFM volume analysis should be applied for relative comparisons among the molecules in high-resolution and high-quality AFM images acquired using an identical AFM tip. However, if some AFM tips must be used to obtain enough data for statistical analysis, high-resolution and high-quality images are required for the analyses at least. In any case, relative comparisons are appropriate for such analyses but not absolute evaluations to avoid the influence of tip geometry. We analyzed the molecular volumes based on these criteria in the present study. The mass center position of a PZ molecule was calculated using the X, Y, and Z coordinates of pixels in the ROI.

The contour length of the bZIP-linker region was analyzed using the following procedure. First, the ROI of a PZ monomer region was determined. Second, a skeleton line was calculated in the ROI so that the distance to the border was the same on both sides of the skeleton line[57]. Third, the height profiles along the skeleton line were displayed as shown in Supplementary Fig. 8. In this profile, the domain boundary in a PZ molecule were determined by the half-maximum height. We then defined the upper and lower side of the boundary as the LOV

domain and the bZIP-linker region, respectively. Finally, the length of the skeleton line in the bZIP-linker region was analyzed as the contour length of the bZIP-linker region.

Data availability

The complete amino acid sequence of PZ was deposited in the DDBJ database (accession number LC629158). The data that support the findings of this study are available from the corresponding author upon reasonable request.

Received: 9 April 2022; Accepted: 21 July 2022
Published online: 08 August 2022

References

1. Lambert, S. A. *et al.* The human transcription factors. *Cell* **172**, 650–665 (2018).
2. Wingender, E., Schoeps, T., Haubrock, M., Krull, M. & Dönitz, J. TFClass: expanding the classification of human transcription factors to their mammalian orthologs. *Nucleic Acids Res.* **46**, D343–D347 (2018).
3. Latchman, D. S. Transcription factors: an overview. *Int. J. Biochem. Cell Biol.* **29**, 1305–1312 (1997).
4. Amoutzias, G. D., Robertson, D. L., Van de Peer, Y. & Oliver, S. G. Choose your partners: dimerization in eukaryotic transcription factors. *Trends Biochem. Sci.* **33**, 220–229 (2008).
5. Todeschini, A. L., Georges, A. & Veitia, R. A. Transcription factors: specific DNA binding and specific gene regulation. *Trends Genet.* **30**, 211–219 (2014).
6. Ellenberger, T. E., Brandl, C. J., Struhl, K. & Harrison, S. C. The GCN4 basic region leucine zipper binds DNA as a dimer of uninterrupted helices : crystal structure of the protein-DNA complex. *Cell* **71**, 1223–1237 (1992).
7. Georges, A. B., Benayoun, B. A., Caburet, S. & Veitia, R. A. Generic binding sites, generic DNA-binding domains: where does specific promoter recognition come from?. *FASEB J.* **24**, 346–356 (2010).
8. Carey, M., Kakidani, H., Leatherwood, J., Mostashari, F. & Ptashne, M. An amino-terminal fragment of GAL4 binds DNA as a dimer. *J. Mol. Biol.* **209**, 423–432 (1989).
9. Hong, M. *et al.* Article structural basis for dimerization in DNA recognition by Gal4. *Structure* **16**, 1019–1026 (2008).
10. Partch, C. L. & Gardner, K. H. Coactivator recruitment: a new role for PAS domains in transcriptional regulation by the bHLH-PAS family. *J. Cell. Physiol.* **223**, 553–557 (2010).
11. Wu, D., Potluri, N., Lu, J., Kim, Y. & Rastinejad, F. Structural integration in hypoxia-inducible factors. *Nature* **524**, 303–308 (2015).
12. Crosson, S., Rajagopal, S. & Moffat, K. The LOV domain family: Photoresponsive signaling modules coupled to diverse output domains. *Biochemistry* **42**, 2–10 (2003).
13. Salomon, M., Christie, J. M., Knieb, E., Lempert, U. & Briggs, W. R. Photochemical and mutational analysis of the FMN-binding domains of the plant blue light receptor, phototropin. *Biochemistry* **39**, 9401–9410 (2000).
14. Takahashi, F. *et al.* AUREOCHROME, a photoreceptor required for photomorphogenesis in stramenopiles. *Proc. Natl. Acad. Sci. USA* **104**, 19625–19630 (2007).
15. Takahashi, F. Blue-light-regulated transcription factor, aureochrome, in photosynthetic stramenopiles. *J. Plant Res.* **129**, 189–197 (2016).
16. Matiiv, A. B. & Chekunova, E. M. Aureochromes: blue light receptors. *Biochemistry* **83**, 662–673 (2018).
17. Hisatomi, O., Nakatani, Y., Takeuchi, K., Takahashi, F. & Kataoka, H. Blue light-induced dimerization of monomeric aureochrome-1 enhances its affinity for the target sequence. *J. Biol. Chem.* **289**, 17379–17391 (2014).
18. Nakatani, Y. & Hisatomi, O. Molecular mechanism of photozipper, a light-regulated dimerizing module consisting of the bZIP and LOV domains of aureochrome-1. *Biochemistry* **54**, 3302–3313 (2015).
19. Kobayashi, I., Nakajima, H. & Hisatomi, O. Molecular mechanism of light-induced conformational switching of the LOV domain in aureochrome-1. *Biochemistry* **59**, 2592–2601 (2020).
20. Hisatomi, O. *et al.* Blue light-induced conformational changes in a light-regulated transcription factor, aureochrome-1. *Plant Cell Physiol.* **54**, 93–106 (2013).
21. Herman, E., Sachse, M., Kroth, P. G. & Kottke, T. Blue-light-induced unfolding of the Jα helix allows for the dimerization of aureochrome-LOV from the diatom phaeodactylum tricornutum. *Biochemistry* **52**, 3094–3101 (2013).
22. Herman, E. & Kottke, T. Allosterically regulated unfolding of the A′α helix exposes the dimerization site of the blue-light-sensing aureochrome-lov domain. *Biochemistry* **54**, 1484–1492 (2015).
23. Heintz, U. & Schlichting, I. Blue light-induced LOV domain dimerization enhances the affinity of aureochrome 1a for its target DNA sequence. *Elife* **5**, 1–21 (2016).
24. Nakajima, H., Kobayashi, I., Adachi, Y. & Hisatomi, O. Transmission of light signals from the light-oxygen-voltage core via the hydrophobic region of the β-sheet surface in aureochrome-1. *Sci. Rep.* **11**, 1–10 (2021).
25. Mitra, D., Yang, X. & Moffat, K. Crystal structures of aureochrome1 LOV suggest new design strategies for optogenetics. *Structure* **20**, 698–706 (2012).
26. Banerjee, A., Herman, E., Kottke, T. & Essen, L.-O. Structure of a native-like aureochrome 1a LOV domain dimer from phaeodactylum tricornutum. *Structure* **24**, 171–178 (2016).
27. Banerjee, A. *et al.* Allosteric communication between DNA-binding and light-responsive domains of diatom class I aureochromes. *Nucleic Acids Res.* **44**, 5957–5970 (2016).
28. Ando, T. *et al.* A high-speed atomic force microscope for studying biological macromolecules. *Proc. Natl. Acad. Sci.* **98**, 12468–12472 (2001).
29. Ando, T., Uchihashi, T. & Scheuring, S. Filming biomolecular processes by high-speed atomic force microscopy. *Chem. Rev.* **114**, 3120–3188 (2014).
30. Ando, T. High-speed atomic force microscopy and its future prospects. *Biophys. Rev.* **10**, 285–292 (2018).
31. Miyagi, A. *et al.* Visualization of intrinsically disordered regions of proteins by high-speed atomic force microscopy. *Chemphyschem* **9**, 1859–1866 (2008).
32. Hashimoto, M. *et al.* Phosphorylation-coupled intramolecular dynamics of unstructured regions in chromatin remodeler FACT. *Biophys. J.* **104**, 2222–2234 (2013).
33. Kodera, N. *et al.* Structural and dynamics analysis of intrinsically disordered proteins by high-speed atomic force microscopy. *Nat. Nanotechnol.* **16**, 181–189 (2021).
34. Wang, X., Chen, X. & Yang, Y. Spatiotemporal control of gene expression by a light-switchable transgene system. *Nat. Methods* **9**, 266–269 (2012).
35. Raghavan, G., Hidaka, K., Sugiyama, H. & Endo, M. Direct observation and analysis of the dynamics of the photoresponsive transcription factor GAL4. *Angew. Chemie - Int. Ed.* **58**, 7626–7630 (2019).
36. Nakatani, Y. & Hisatomi, O. Quantitative analyses of the equilibria among DNA complexes of a blue-light-regulated bZIP module. *Photozipper. Biophys. Physicobiology* **15**, 8–17 (2018).

37. Weiss, M. A. *et al.* Folding transition in the DNA-binding domain of GCN4 on specific binding to DNA. *Nature* **347**, 575–578 (1990).
38. Richards, J. P., Bächinger, H. P., Goodman, R. H. & Brennan, R. G. Analysis of the structural properties of cAMP-responsive element-binding protein (CREB) and phosphorylated CREB. *J. Biol. Chem.* **271**, 13716–13723 (1996).
39. Saxton, M. J. Single-particle tracking: the distribution of diffusion coefficients. *Biophys. J.* **72**, 1744–1753 (1997).
40. Stetefeld, J., McKenna, S. A. & Patel, T. R. Dynamic light scattering: a practical guide and applications in biomedical sciences. *Biophys. Rev.* **8**, 409–427 (2016).
41. Akiyama, Y., Nakasone, Y., Nakatani, Y., Hisatomi, O. & Terazima, M. Time-resolved detection of light-induced dimerization of monomeric aureochrome-1 and change in affinity for DNA. *J. Phys. Chem. B* **120**, 7360–7370 (2016).
42. Milo, R. & Phillips, R. *Cell Biology by the Numbers.* (Garland Science, 2015).
43. Biggin, M. D. Animal transcription networks as highly connected quantitative continua. *Dev. Cell* **21**, 611–626 (2011).
44. Kribelbauer, J. F., Rastogi, C., Bussemaker, H. J. & Mann, R. S. Low-affinity binding sites and the transcription factor specificity paradox in eukaryotes. *Annu. Rev. Cell Dev. Biol.* **35**, 357–379 (2019).
45. Saudek, V. *et al.* The solution structure of a leucine-zipper motif peptide. *Protein Eng. Des. Sel.* **4**, 519–529 (1991).
46. Pérez, J., Vachette, P., Russo, D., Desmadril, M. & Durand, D. Heat-induced unfolding of neocarzinostatin, a small all-β protein investigated by small-angle X-ray scattering. *J. Mol. Biol.* **308**, 721–743 (2001).
47. Hakoshima, T. Leucine Zippers. *eLS* https://doi.org/10.1002/9780470015902.a0005049.pub2 (2014).
48. Miller, M. The importance of being flexible: the case of basic region leucine zipper transcriptional regulators. *Curr. Protein Pept. Sci.* **10**, 244–269 (2009).
49. Shoemaker, B. A., Portman, J. J. & Wolynes, P. G. Speeding molecular recognition by using the folding funnel: the fly-casting mechanism. *Proc. Natl. Acad. Sci.* **97**, 8868–8873 (2000).
50. Pufall, M. A. & Graves, B. J. Autoinhibitory domains: modular effectors of cellular regulation. *Annu. Rev. Cell Dev. Biol.* **18**, 421–462 (2002).
51. Wang, X. *et al.* Dynamic autoinhibition of the HMGB1 protein via electrostatic fuzzy interactions of intrinsically disordered regions. *J. Mol. Biol.* **433**, 167122 (2021).
52. Huebner, K., Procházka, J., Monteiro, A. C., Mahadevan, V. & Schneider-Stock, R. The activating transcription factor 2: an influencer of cancer progression. *Mutagenesis* **34**, 375–389 (2019).
53. Bhoumik, A., Lopez-bergami, P. & Ronai, Z. ATF2 on the double: activating transcription factor and DNA damage response protein. *Pigment Cell Res.* **20**, 498–506 (2007).
54. Williams, S. C., Baer, M., Dillner, A. J. & Johnson, P. F. CRP2 (C/EBP beta) contains a bipartite regulatory domain that controls transcriptional activation, DNA binding and cell specificity. *EMBO J.* **14**, 3170–3183 (1995).
55. Lynch, V. J., May, G. & Wagner, G. P. Regulatory evolution through divergence of a phosphoswitch in the transcription factor CEBPB. *Nature* **480**, 383–386 (2011).
56. Yamashita, H. *et al.* Role of trimer-trimer interaction of bacteriorhodopsin studied by optical spectroscopy and high-speed atomic force microscopy. *J. Struct. Biol.* **184**, 2–11 (2013).
57. Kimmel, R., Shaked, D., Kiryati, N. & Bruckstein, A. M. Skeletonization via distance maps and level sets. *Comput. Vis. Image Underst.* **62**, 382–391 (1995).

Acknowledgements

This work was supported by JSPS KAKENHI Grant Numbers 20H03223, 22K18945 (to H.Y.) and 19K06586 (to O.H.), and 19H05789, 21H01812, 21K18876 (to M.A.), PRESTO, JST JPMJPR15FD, Multidisciplinary Research Laboratory System of Osaka University, the Osaka University Program for the Support of Networking among Present and Future Researchers, the joint research program of Biosignal Research Center, Kobe University 192005, and Takeda Science Foundation (to H.Y.). The authors thank Forte (www.fortescience.com) for English language editing.

Author contributions

H.Y. and O.H. conceptualized the study. A.T. and H.Y. designed the experiments. O.H prepared the protein samples. A.T. and H.Y. performed the HS-AFM experiments and analyzed the results. H.Y., O.H. and M.A. administrated and supervised the study. A.T. and H.Y. wrote the main manuscript text. All authors reviewed the final version of the manuscript.

Competing interests

The authors declare no competing interests.

Additional information

Supplementary Information The online version contains supplementary material available at https://doi.org/10.1038/s41598-022-17228-6.

Correspondence and requests for materials should be addressed to H.Y.

Reprints and permissions information is available at www.nature.com/reprints.

Publisher's note Springer Nature remains neutral with regard to jurisdictional claims in published maps and institutional affiliations.